Elucidation of Complex Triplet Excited State Dynamics in Pd(II) Biladiene Tetrapyrroles

Shea M. Martin,[1] Gil Repa,[1] Robert C. Hamburger,[1] Craig Pointer,[1] Kaytlin Ward,[2] Trong-Nhan Pham,[2] Maxwell I. Martin,[2] Joel Rosenthal,[2*] Lisa A. Fredin,[1*] Elizabeth R. Young[1*]

[1] Department of Chemistry, Lehigh University, 6 E. Packer Ave., Bethlehem, PA 18015, USA.
[2] Department of Chemistry and Biochemistry, Brown Laboratory, University of Delaware, Newark, DE 19716, United States

Keywords: Transient absorption spectroscopy, mechanistic studies, density functional theory, triplet formation, metal-centered triplet, porphyrinoid, tetrapyrrole macrocycles.

Pd(II) biladienes have been developed over the last five years as *non-aromatic* oligotetrapyrrole complexes that support a rich triplet photochemistry. In this work, we have undertaken the first detailed photophysical interrogation of three homologous Pd(II) biladienes bearing different combinations of methyl- and phenyl-substituents on the frameworks' sp^3-hybridized *meso*-carbon (*i.e.*, the 10-position of the biladiene framework). These experiments have revealed unexpected excited-state dynamics that are dependent on the wavelength of light used to excite the biladiene. More specifically, transient absorption spectroscopy revealed that higher-energy excitations (λ_{exc} ~ 350-500 nm) led to an additional lifetime *(i.e.*, an extra photophysical process) compared to experiments carried out following excitation into the lowest-energy excited states (λ_{exc} = 550 nm). Each Pd(II) biladiene complex displayed an intersystem crossing lifetime on the order of tens of ps and a triplet lifetime of ~20 μs, regardless of the excitation wavelength. However, when higher-energy light is used to excite the complexes, a new lifetime on the order of hundreds of ps is observed. The origin of the 'extra' lifetime observed upon higher energy excitation of the Pd(II) biladiene complexes was revealed by detailed computational modeling using density functional theory (DFT) and time-dependent DFT (TDDFT). These efforts demonstrated that excitation into higher-energy metal-mixed-charge-transfer excited states with high spin-orbit coupling to higher energy metal-mixed-charge-transfer triplet states leads to the additional excitation deactivation pathway. Importantly, time-resolved spectroscopy and electronic structure calculations carried out for the analogous *aromatic* Pd(II) meso-tetrakis(pentafluorophenyl)porphyrin (**Pd[TPFPP]**) demonstrated this traditional tetrapyrrole does not display the excitation-wavelength dependent photophysics observed for the Pd(II) biladienes. These experiments confirm that the unusual photophysics we observe are unique to low-symmetry biladienes and do not apply to more well-studied porphyrinoids. The results of this work demonstrate that Pd(II) biladienes support a unique triplet photochemistry that may be exploited for development of new photochemical schemes and applications.

Introduction

Porphyrins and related tetrapyrrole macrocycles support a rich photochemistry that make them appealing for a range of applications.[1,2] While a great deal is known about porphyrins and their photochemistry, much less is known about the photochemistry and photophysics of related *non-aromatic* tetrapyrrole architectures such as isocorroles,[3,4,5–7,8,9] phlorins,[10,11–15,16] and biladienes.[17] Each of these less traditional architectures contains an sp^3-hybridized *meso*-carbon, which breaks the cyclic conjugation of the tetrapyrrole motif. Further, biladienes are oligotetrapyrroles and are not macrocyclic. These structural modifications ablate the tetrapyrrole aromaticity and dramatically alter the electronic structure of these species, leading to unusual and exciting spectroscopic, redox and photochemical properties.

10,10-Disubstituted biladiene complexes (such as those shown in Figure 1) are of much lower symmetry as compared to traditional aromatic porphyrins. The disruption of π-conjugation imparted by the sp^3-hybridized 10-position and the non-macrocyclic nature of the tetrapyrrole gives rise to several attractive properties as compared to traditional porphyrinoids, including (1) biladienes are facile to synthesize and numerous synthetic modifications (*i.e.* addition of substituents to various positions on the biladiene) can be achieved to create a diverse set of derivatives; (2) metalated biladienes have light absorption profiles that support photochemical applications using visible to near-IR light; and (3) inclusion of heavy metals, like Pt or Pd promotes rapid intersystem crossing (ISC) and long lived triplet

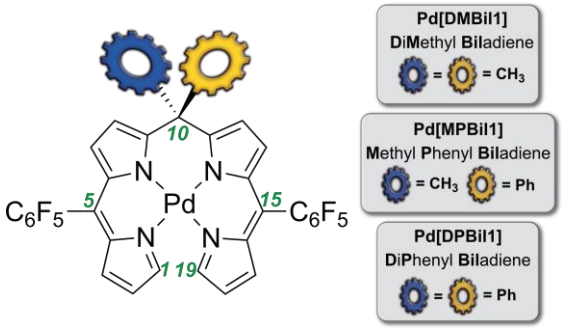

Figure 1. Pd(II)-biladiene complex series bearing different combinations of methyl- and phenyl-substituents at the sp^3-hybridized *meso*-carbon (*i.e.*, the 10-position of the biladiene framework): geminal dimethyl substituents a the 10-position (**Pd[DMBil1]**), geminal methyl and phenyl substituents (**Pd[MPBil1]**) and geminal diphenyl groups (**Pd[DPBil1]**).

excited states, which is requisite for photodynamic therapy and other applications that utilize triplet photosensitizers.[17,18,19,20,21,22,23] Indeed, previous work in our groups has demonstrated the viability of a series of Pd(II) biladiene moieties (Figure 1) for singlet oxygen sensitization using long-visible and NIR light from within the so-called phototherapeutic window (~600-900 nm).[17,24,25,26,27] Up until this point, however, the excited-state dynamics of biladiene complexes, as well as that of related *non-aromatic* tetrapyrroles have remained virtually unexplored.

In contrast, a great deal is known about porphyrin photophysics. For typical photophysics observed for porphyrins, the number of lifetimes and the dynamics of the excited state evolution do not depend on the excitation wavelength. In general, excitation of porphyrins into higher energy excited states results in rapid nonradiative internal conversion (IC) to the lowest-energy singlet. From this state, relaxation to the ground state may occur radiatively or non-radiatively. In porphyrins containing heavy metals, like Pt or Pd, intersystem crossing (ISC) to low-lying, long-lived triplet states is efficient and is followed by deactivation to the ground state.

Relatively few reports exist in which the excited-state dynamics of porphyrins show excitation-wavelength dependence. For example, prior work utilizing transient absorption spectroscopy to measure the excited-state dynamics of freebase porphyrins reported a very short (0.7 ps) lifetime when excited into the Soret band that is not observed upon longer wavelength excitation into the Q bands.[28] These and several other very short (< 1 ps) wavelength-dependent lifetimes in porphyrinoids have been attributed to a nonradiative internal conversion (IC) from higher-lying singlet states to the lowest singlet excited state.[29] The lowest-energy singlet state then undergoes intersystem crossing (ISC) with the same time constant observed upon direct excitation into the lowest-energy singlet state (*i.e*., excitation into the Q-bands). Additionally, porphyrins containing first row transition metals are known to undergo rapid, vibrationally excited *d-d* transitions between singlet and triplet states that show moderate excitation-wavelength dependent dynamics.[30-31] Certain nickel porphyrins, such as Ni(OEP) (OEP = octaethylporphyrin) can exhibit wavelength-dependent photophysics involving metal-centered, vibrationally-excited singlet states rapidly (sub-ps) converting to triplet *d*-centered states. These metal-centered triplet states, which are dominated by *d-d* transitions, undergo nonradiative deactivation via the lowest-lying triplet state in several hundred ps. In general, the few reports in which wavelength dependent photophysics have been observed for porphyrins have involved relatively small changes to ps-timescale vibrational cooling or the introduction of internal conversion processes from higher lying excited states within a singlet manifold.

In exploring the photochemistry of *non-aromatic* tetrapyrroles, we became curious about which aspects of biladiene photophysics might be the same (or different) from those observed for well-studied porphyrins systems. In initial work, we reported the excited-state dynamics for the series of Pd(II) biladiene derivatives shown in Figure 1. Using transient absorption spectroscopy, we found that excitation into the lowest-energy absorption feature of Pd(II) biladiene complexes (representing excitation in to the S_1 and S_2 states) produced straightforward photophysics similar to what has been observed previously for Pd(II) porphyrins, which consisted of a single lifetime on the picosecond timescale corresponding to singlet to triplet evolution, followed by a longer lifetime on the microsecond time range corresponding to decay of the triplet state.[32]

Building on these initial transient absorption experiments, we have undertaken more detailed efforts to map the photophysics of the **Pd[DMBil1]**, **Pd[MPBil1]**, and **Pd[DPBil1]** biladiene complexes of Figure 1. In expanding our photophysical work, we discovered excitation into higher-lying excited states resulted in the appearance of a third lifetime upon TA analysis. The origin of this third lifetime, which has not to the best of our knowledge been previously observed for any other Pd(II) tetrapyrroles, required additional efforts including insights gained from theory to fully understand and interpret.

In this work, we combine transient absorption spectroscopy (TAS), bolstered by steady-state and time-resolved emission spectroscopy, and density functional theory (DFT) to provide intuition into the origin of an unexpected third lifetime that is observed at higher excitation energies. In addition to providing full TAS analysis for the three Pd(II) biladienes of Figure 1 upon excitation at three different energies, DFT carried out on the dimethyl version (**Pd[DMBil1]**) provides a rationalization for the observed photophysics. Comparison of the results obtained for **Pd[DMBil1] Pd[MPBil1]**, and **Pd[DPBil1]** to those for a homologous Pd(II) porphyrin (**Pd[TPFPP]**) reveal that the excitation wavelength-dependent behavior is unique to biladiene complexes. The combination of spectroscopy and theory presented herein provide a framework to understand the intriguing and unexpected excited-state evolution of these molecular systems.

Experimental methods

Sample preparation. Synthesis and characterization of the Pd(II) biladiene series were carried out and reported previously.[32] Synthesis and characterization of the **Pd[TPFPP]** was carried out according to literature precedent.[33] Samples for emission spectroscopy were prepared using spectroscopic grade methanol from Sigma Aldrich. Samples for TAS were prepared under high vacuum in a 2−mm quartz cuvettes. Samples were prepared to known concentrations ranging between 20−50 μM and were subjected to at least 3 cycles of freeze-pump-thaw to ensure the samples were degassed.

UV-visible absorption spectroscopy. UV-visible absorption spectra were collected on an OceanOptics diode array spectrometer (Flame-S series) before and after acquisition of TAS data to ensure that no decomposition occurred. Samples were found to be stable under laser illumination over the course of the experiments.

Emission spectroscopy. Steady-state emission spectroscopy was carried out on an ISS Chronos BH with steady-state upgrade. Samples for steady-state emission spectroscopy were prepared using spectroscopic-grade methanol. The solvent (1 mL) was transferred to prepared dried aliquots and the sample was transferred to a high-vacuum cuvette with pathlength of 0.4 cm. Samples were degassed using freeze–pump–thaw techniques to ensure that no oxygen was present in the samples. Samples were excited between 370-550 nm starting with 370 nm excitation and progressing in 10 nm increments until (and

including) 550 nm excitation. Emission was collected beginning 20 nm to the red of excitation to 800 nm with 1 nm step-size and 1-second integration time. Excitation spectra were recorded by monitoring the emission at 550 nm, 560 nm, 590 nm, 610 nm, and 710 nm while exciting at wavelengths 350 nm to 20 nm blue of monitored emission in 1 nm step-size and 1-second integration time.

Transient absorption spectroscopy. Transient absorption spectroscopy was carried out using a Helios/EOS system from Ultrafast systems with excitation provided by a Coherent Libra and has been described elsewhere.[34] A Topas-C optical parametric amplifier was used to generate the excitation wavelengths of a 350 nm, 490 nm, and 570 nm. The pump pulse was attenuated to 0.4 mW to prevent decomposition of the sample. The femtosecond transient absorption (fs-TAS) spectra were measured over a 5 ns window. For each scan, 250 time points were recorded and each sample was subjected to three scans that were averaged to produce the final data set. At least three samples were recorded for each biladiene and **Pd[TPFPP]** moiety. Nanosecond transient absorption spectroscopy (ns-TAS) was performed using and Ultrafast Systems EOS spectrometer. The pump pulses were the same as those used in the femtosecond TA experiment. The white light for the probe beam is generated using fiber optic laser, specifically a pulsed PCF-based laser. Time windows for nanosecond TAS ranged between 30 – 100 μs, depending on the bildiene moiety. Time delays in the nanosecond TAS experiment are sampled randomly using an electronically controlled delay.

Data analysis for the fs-TAS data was performed using principal component analysis via singular value decomposition. For each sample, two principal components (PC) were found to represent the data well. Fitting to these PC was completed using global lifetime analysis (GLA) software (Ultrafastsystems Surface Xplorer) to isolate decay-associated difference spectra (DADS) and their corresponding lifetimes. In every set of fs-TAS data, either two or three lifttimes were found to fit the data, with one of the lifetimes being too long to resolve on the 5-ns window accessible on the fs-TAS experiment. The longest lifetime was allowed to fit as "infinite" on that time scale. The "infinite" lifetime was determined using single wavelenth fitting of the ns-TAS data at triplet aboroption peak ~680 nm. The triplet lifetime obtained from this fitting is shown as the lifetime of the longest-lived DADS in GLA results.

Density functional theory. Density functional theory (DFT) was used to understand the electronic structure of **Pd[DMBil1]** for simplicity. Structures were optimized using a hybrid functional M06-L which is particularly good for energetics of transition metal complexes and triple-ζ basis sets: all electron 6-311G(d,p) for light atoms (H,C,N) and an effective core potential (ECP), LANL2DZ on Pd; with a polarizable continuum model (PCM) of MeOH solvation level in Gaussian 09[35]. Spectra are plotted with a wavelength correction factor of 0.95.[36]

Time-dependent density functional theory (TDDFT) was used to calculate both the triplet and singlet excited states of **Pd[DMBil1]** using the same level of theory as for DFT. In addition, the one-electron Z_{eff} spin-orbit couplings were tabulated using a modified PySOC[37] where the Pd^{2+} was assigned a Z_{eff} = 232.[38]

Results and discussion

Mechanistic overview of Pd(II) biladienes and Pd[TPFPP] photophysics. All three of the Pd(II) biladiene (**Pd[DMBil1]**, **Pd[MPBil1]**, and **Pd[DPBil1]**) complexes studied in this work show similar photophysical behavior that is excitation-wavelength dependent and are distinct from more traditional Pd(II) tetrapyrroles.

Transient absorption spectroscopy reveals that at low-energy excitation (~570 nm), two lifetimes are observed (τ_1 = ~10-15 ps ; τ_3 = ~20 μs). In contrast, upon higher-energy excitation (~350 nm) a third lifetime is needed to fit the photophysical data. The "additional" lifetime (τ_2) observed at higher-energy excitation fits to an intermediate lifetime (hundreds of ps) compared to the other two lifetimes (~ tens of ps and tens of μs). Each of the lifetimes remain relatively consistent for each of the biladiene complexes regardless of excitation energy. While the presence of the τ_2 lifetime is clear from the DADS analysis, its photophysical origin was not immediate apparent and has been the focus of interrogation in this study. In addition, the emission excitation spectrum does not reproduce the absorption spectrum when collected at any emission wavelength. Specifically, the most prominent peak in the absorption spectrum at ~480 nm appears to lead to little emission intensity in the excitations scans (Figure S12). These unexpected emission excitation spectra bolster the observation that the Pd(II) biladienes support atypical photophysics.

To confirm this point, we also probed the photophysics for the aromatic **Pd[TPFPP]** porphyrin complex. These experiments revealed standard photophysical behavior for the aromatic tetrapyrrole homolog; no excitation-wavelength dependence was observed for the emission spectroscopy of **Pd[TPFPP]** and the emission excitation scan reproduced the absorption spectrum. Further, TAS carried out for **Pd[TPFPP]** revealed typical photophysics in which the value and number of lifetimes do not vary with excitation wavelength. As summarized in Scheme 1, excitation in the lowest energy excited state (550 nm) as well as higher excited states (400 nm and 380 nm) result in rapid conversion to the lowest-energy singlet excited

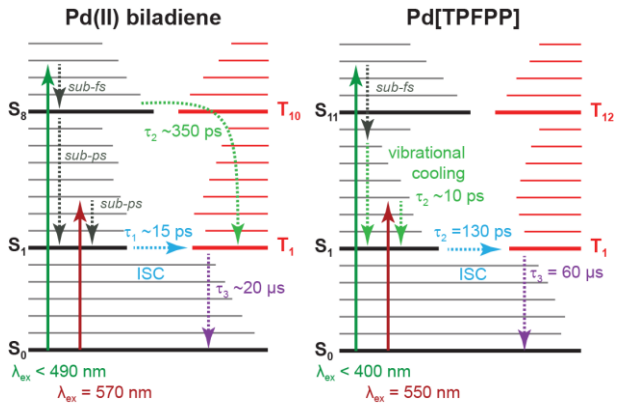

Scheme 1. Jablonski diagram summarizing the excitation wavelength dependent excited-state dynamics of the Pd(II) biladienes.

state (~10 ps), intersystem crossing (~130 ps) to the triplet state, followed by decay of the triplet state (60μs).

Density functional theory provided better understanding of the origin of the distinct photophysics (which are summarized in Table 1 and Scheme 1) observed for **Pd[DMBil1]** **Pd[MPBil1]**, and **Pd[DPBil1]** as compared to those for the **Pd[TPFPP]** porphyrin. To summarize our findings, which are discussed in depth in the section that follows, excitations that result in ligand-centered excited states result in more typical photophysics that evolve quickly to the lowest-lying singlet excited state, which can either result in singlet emission from the S_1 state with only weak spin-orbit coupling to the lower lying triplet excited states. However, higher-energy excitations that result in charge-transfer excited states in the Pd(II) biladienes possess significant spin-orbit coupling to higher-lying mixed-metal-charge-transfer (MMCT) triplet states (T_n, where n > 1). Excitation into the charge-transfer excited states therefore results in dark states which deactivate through the lowest energy triplet back to the ground state. In particular, the broken symmetry of the biladiene seems to lead to stronger interaction between the Pd(II) center and the tetrapyrrole ligand, which facilitates population of the relatively low energy MMCT excited states in both the singlet and triplet manifolds, and leads to the interesting wavelength dependence in the photophysics observed.

UV-visible absorption spectroscopy. Figure 2 shows the absorption spectra of **Pd[DMBil1]**, **Pd[MPBil1]**, and **Pd[DPBil1]** in dried, degassed methanol. The three biladienes show very similar absorption features in the UV region. In the visible region, each biladiene displays a large Soret-like peak centered at ~480 nm with a smaller, relatively sharp peak centered at ~550 nm.

Transient absorption spectroscopy (TAS): representative spectra and global analysis on Pd(II) biladienes. Figure

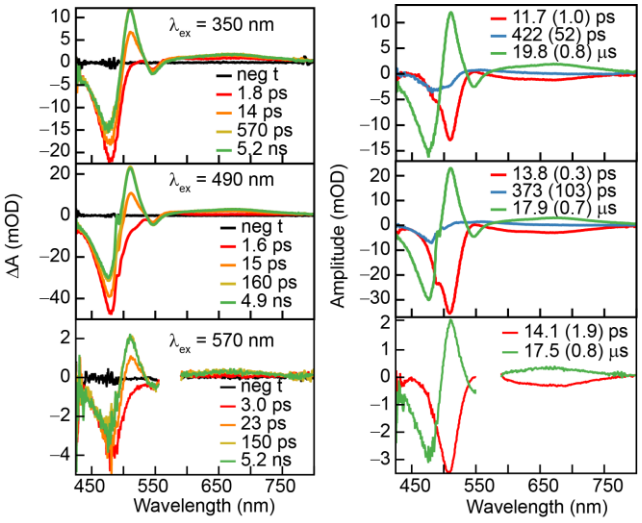

Figure 3. Transient absorption data and analysis of **Pd[DMBil1]** upon excitation at 350 nm, 490 nm and 570 nm. (left column) Representative spectra of **Pd[DMBil1]** upon excitation at different wavelengths. (right column) Decay-associated difference spectra (DADS) produced upon global analysis fitting of each data set. Samples were prepared using freeze-pump-thaw to degas the samples in dried methanol. Gaps in signal correspond to scattering of excitation light.

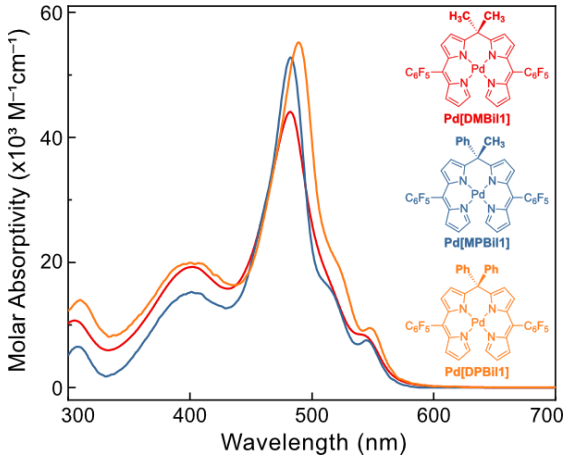

Figure 2. UV-Visible absorption spectra of **Pd[DMBil1]**, **Pd[DMBil1]**, and **Pd[DMBil1]** recorded in dry, degassed methanol.

3 shows TAS representative spectra (left column) along with the corresponding global analysis decay-associated difference spectra (DADS) (right column) recorded for **Pd[DMBil1]** upon excitation at either 350, 490, or 570 nm. The ground-state absorption spectrum for **Pd[DMBil1]** overlaid onto the TAS representative spectra is shown in Figure S1. The representative spectra show a large bleach at 480 nm and a smaller bleach at 550 nm convolved with a growth at 510 nm that appears over the first several nanoseconds. An additional broad growth appears over the first several nanoseconds between ~560-750 nm. The bleaches at 480 and 550 nm can be assigned to loss of the **Pd[DMBil1]** ground state upon comparison to the overlaid spectra in Figure S1. The induced absorptions that appear at 510 nm and 560-750 nm persist for ~100 μs suggesting that they represent formation of a long-lived triplet excited state.

*Global analysis fitting and decay-associated difference spectra (DADS) of **Pd[DMBil1]***. Global analysis was performed to determine the number of components contributing to the excited-state evolution of **Pd[DMBil1]** and to obtain lifetimes for each component. Consistent with our prior work, global analysis revealed that when **Pd[DMBil1]** is excited into its lowest-energy electronic transition at 570 nm, two DADS with lifetimes of τ_1 = 14.1 ps and τ_3 = 17.5 μs are obtained (Note that all μs lifetimes reported in this section are obtained from fitting ns-TAS data as described in the Experimental section and reported in the *Nanosecond TAS of Pd(II) Biladienes* section below). These lifetimes are presumed to correspond to the singlet to triplet transition (τ_1) and the lifetime of the triplet excited state (τ_3).

Notably, when **Pd[DMBil1]** is excited at higher energies (*i.e.*, at either 350 nm or 490 nm) resulting in population of higher-lying excited states, three lifetimes are obtained upon global analysis fitting. Two of the DADS and their corresponding lifetimes match those obtained upon lower-energy excitation (τ_1 = ~14 ps and τ_3 = 17-19 μs). The third DADS grows in amplitude with increasing excitation energy, and fits to an intermediate lifetime of τ_2 = 373 ps upon excitation at 490 nm and τ_2 = 422 ps upon excitation at 350 nm. A good quality of fit is obtained from the global analysis (Figure S2) as shown with

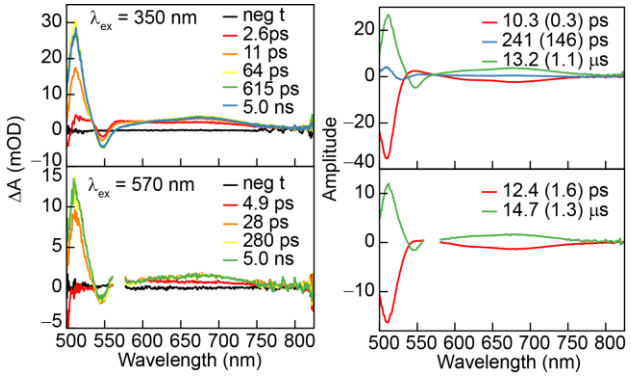

Figure 4. Transient absorption data and analysis of MP upon excitation at 350 nm and 570 nm. (left column) Representative spectra of **Pd[MPBil1]** upon excitation at different wavelengths. (right column) Decay-associated difference spectra (DADS) produced upon global analysis fitting of each data set. Samples were prepared using freeze-pump-thaw to degas the samples in dried methanol. Gaps in signal correspond to scattering of excitation light.

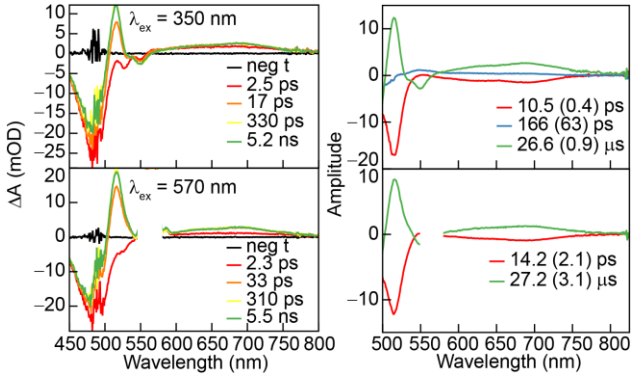

Figure 5. Transient absorption data and analysis of DP upon excitation at 350 nm and 570 nm. (left column) Representative spectra of **Pd[DPBil1]** upon excitation at different wavelengths. (right column) Decay-associated difference spectra (DADS) produced upon global analysis fitting of each data set. Samples were prepared using freeze-pump-thaw to degas the samples in dried methanol.

principal kinetic traces. All lifetimes are summarized in Table 1.

Although the amplitude of the additional DADS (τ_2 = 373 ps, λ_{ex} = 490 nm; and τ_2 = 422 ps, λ_{ex} = 350 nm) is relatively small compared to the other two DADS lifetimes, we were unable to fit the global data well with only two DADS. Therefore, we find that this additional lifetime (*i.e.*, τ_2) is indeed needed to represent the data for the higher-energy excitation experiments. Since the origin of this additional lifetime was not immediately clear, computational work as described at the end of the Results and Discussion section was undertaken to shed light on the nature of the new excited state dynamics that are observed upon high energy excitation of **Pd[DMBil1]**.

*TAS and Global analysis fitting of **Pd[MPBil1]** and **Pd[DPBil1]**.* Similar TAS experiments and global analyses were conducted for the other two biladiene complexes of Figure 1 (*i.e.*, **Pd[MPBil1]** and **Pd[DPBil1]**) and produced results similar to those obtained for **Pd[DMBil1]**. The results from the highest (570 nm) and lowest (350 nm) excitation wavelength data are presented in Figure 4 and Figure 5 for **Pd[MPBil1]** and **Pd[DPBil1]**, respectively. TA spectra recorded for **Pd[MPBil1]** show a small bleach at 540 nm, a growth centered at 515 nm, and a large positive feature spanning 560 – 800 nm (Figure 4). Global analysis shows components similar to those observed for **Pd[DMBil1]** (*vide supra*). The data collected for **Pd[MPBil1]** following excitation at 350 nm contained three DADS lifetimes (τ_1 = 10.3 ps; τ_2 = 241 ps; τ_3 = 13.2 μs), while the data for **Pd[MPBil1]** excited at 570 nm contains only two DADS (τ_1 = 12.4 ps; τ_3 = 14.7 μs). TA spectra and global analysis for **Pd[DPBil1]** excited at 350 and 570 nm (Figure 5) show features similar to **Pd[DMBil1]** and **Pd[MPBil1]** in which a large bleach forms immediately at ~480 nm, followed by a growth peak centered at 520 nm and a broad growth feature spanning 600 – 800 nm. Global analysis for **Pd[DPBil1]** shows that the lower excitation wavelength (350 nm) contained three components with lifetimes of τ_1 = 10.5 ps, τ_2 = 166 ps, and τ_3 = 26.6 μs. When excited at lower energy (570 nm), **Pd[DPBil1]** data contained only two components with lifetimes of τ_1 = 14.2 ps and τ_3 = 27.2 μs. When taken as a whole the combined results of the fs-TAS experiments and global analysis demonstrate that

Table 1. Lifetimes for the Pd(II) Biladiene Series and **Pd[TPFPP]** as a Function of Excitation Wavelength

Moiety	λ_{ex} (nm)	τ_1 (ps)	τ_2 (ps)	τ_3 (μs)
Pd[DMBil1]	350	11.7 (1.0)	422 (52)	19.8 (0.8)
	490	13.8 (0.3)	373 (103)	17.9 (0.7)
	570	14.1 (1.9)		17.5 (0.8)
Pd[MPBil1]	350	10.3 (0.3)	241 (146)	13.2 (1.1)
	490	11.5 (0.8)	215 (145)	12.1 (2.3)
	570	12.4 (1.6)		14.7 (1.3)
Pd[DPBil1]	350	10.5 (0.4)	166 (63)	26.6 (0.9)
	490	15.3 (0.3)	280 (190)	30.0 (2.0)
	570	14.2 (2.1)		27.2 (3.1)
Pd[TPFPP]	380	10 (2)	130 (40)	60 (6)
	400	11(0.6)	130 (30)	62 (6)
	550	7.8 (0.6)	132 (42)	62 (7)

Numbers in parentheses are the standard deviation of fitted values.
Note that the origins of the three lifetimes in the Pd(II) biladiene moieties and the **Pd[TPFPP]** are different as described in the relevant sections of the manuscript.

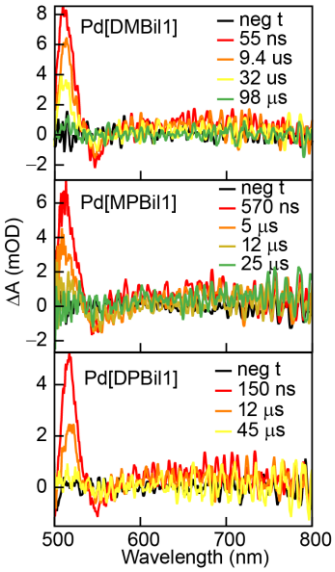

Figure 6. Nanosecond transient absorption representative spectra of **Pd[DMBil1]**, **Pd[DMBil1]**, and **Pd[DMBil1]** upon excitation at 350 nm. Samples were prepared using freeze-pump-thaw to degas the samples in dried methanol.

all three Pd(II) biladiene complexes of Figure 1 support a distinct photophysical process (*i.e.*, τ_2) upon excitation into the higher energy Soret-like band that is not observed upon excitation at lower energies. The Jablonski diagram illustrating these basic photophysical schemes is Shown in Scheme 1.

Nanosecond TAS of Pd(II) Biladienes. Results of ns-TAS for all three Pd(II) biladienes excited at 350 nm (Figure 6) show the continuation of the photophysical evolution of each species from the corresponding fs-TAS data. Similar spectral features to those observed at the end of the fs-TAS temporal window, namely a small bleach at ~550 nm, in addition to a large induced absorption at ~515 nm and weak induced absorption from 600 – 800 nm are present in the ns-TAS data. Heat maps of the ns-TAS data (Figure S3) are shown on nanosecond and microsecond temporal windows to highlight the absorption changes that occur on the ps to ns timescale and to demonstrate that the signal completely returns to the ground state on the microsecond timescale. Kinetic traces of the single-wavelength fitting performed on the ns-TAS data show that a single exponential decay fits the TA signal for each of the Pd(II) biladiene homologs (Figure S4).

Steady-state emission spectroscopy of Pd[DMBil1]. To more fully understand the unusual wavelength-dependent photophysics observed for the three Pd(II) biladienes, we carried out excitation-wavelength dependent emission and excitation scans. The emission spectrum of **Pd[DMBil1]** shows very little change as a function of the excitation wavelength, as is typical for most organic and inorganic luminophores (Figure S11).

The shape of the excitation spectra (Figure 7, solid lines show normalized excitation spectra of **Pd[DMBil1]** over a range of emission wavelengths) is generally invariant to the emission wavelength being monitored. However, the shape of the emission spectra recorded for **Pd[DMBil1]** are distinct as compared to the absorption spectrum recorded for this biladiene complex (overlaid as a black dashed line in Figure 7). The unnormalized excitation scans are shown in Figure S12. The excitation spectra recorded for **Pd[DMBil1]** show two prominent peaks at ~421 nm and ~526 nm. The excitation peak at 421 nm overlaps well with a higher-order excitation corresponding to the absorption spectrum peak at 400 nm. The excitation scan peak at ~526 nm appears to correspond to the lowest lying absorption features (a slight shoulder at ~520 and small peak at 550 nm) of the absorption spectrum. Unexpectedly, the most prominent peak in the absorption spectrum at ~480 nm appears to lead to little emission intensity in the excitations scans.

Steady-state and time-resolved spectroscopy of related Pd[TPFPP] porphyrin moiety. In order to determine if the wavelength-dependent photophysics we observed for the Pd(II) biladienes also occur for more traditional porphyrinoids (despite not being widely reported in prior literature), we carried out excitation-wavelength dependent steady-state and time-resolved spectroscopy on Pd(II) meso-tetrakis(pentafluorophenyl)porphyrin (**Pd[TPFPP]**).[39–43] Notably, **Pd[TPFPP]** is structurally analogous to the Pd(II) biladienes of Figure 1 and therefore represents an excellent aromatic tetrapyrrole complex to contrast to the non-aromatic biladienes.

We first considered the absorption and emission spectra of **Pd[TPFPP]** and found them to be consistent with previous reports.[39] The **Pd[TPFPP]** porphyrin shows absorption peaks at 403 nm (Soret) and at 518 nm and 552 nm (Q-bands) in methanol solution (Figure S13). Emission peaks are observed at 553 nm and 601 nm (fluorescence) and at 668 nm and 735 nm (phosphorescence) (Figure S13).

We next examined the excitation wavelength-dependent steady-state emission of **Pd[TPFPP]**. Emission spectra rec-

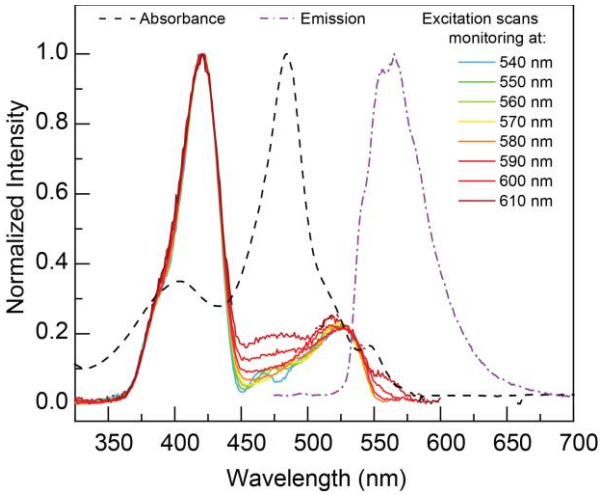

Figure 7. Steady-state absorption (black dashed line), steady-state emission (λ_{ex} = 420 nm, purple dot-dashed line) and normalized excitation scans (solid lines, multiple colors) collected at emission wavelengths across the emission peak of **Pd[DMBil1]** in methanol. The emission intensity is relatively low for the 600 and 620 nm excitation scans, therefore when these scans are normalized and compared to the strongly emitting excitation scans at 550-580 nm extraneous background signal (that may be due to Raman scattering) becomes more prominent.

orded for **Pd[TPFPP]** (shown in Figure S14) do not show a dependence on excitation wavelength. Further, excitation spectra monitored across the porphyrin's entire range of emission wavelengths are well matched to the absorption spectrum of **Pd[TPFPP]** (Figure S15). Accordingly, **Pd[TPFPP]** demonstrates well-behaved and expected steady-state emission, unlike that detailed for the series of Pd(II) biladienes studied herein (*vide supra*).

We then carried out TAS with the goal of determining if the number of excited state lifetimes of **Pd[TPFPP]** varies as a function of excitation wavelength. Excitation at 550 nm (representing excitation into the lowest-lying, S_1 state), and at 400 nm and at 380 nm (different energies within the Soret band that lead to excitation into higher S_n states) were chosen to probe the dynamics of **Pd[TPFPP]**. fs-TAS and ns-TAS representative spectra for each excitation wavelength are relatively consistent (Figures S16 and S17, respectively). For each excitation wavelength the best fitting of the data resulted in three lifetimes: $\tau_1 \sim$ 10 ps, $\tau_2 \sim$ 130 ps and $\tau_3 \sim$ 60 μs (summarized in Figure S16). The shortest two lifetimes (τ_1 and τ_2) result from rapid solvent reorganization, internal conversion, and fast ISC to the triplet state.[28,44–46] Within the standard experimental variation, neither the values nor the number of lifetimes representing the best fits of the data varied as a function of excitation wavelength. This invariance is expected for chromophores that display typical photophysical evolution.

Detailed global analysis fitting was carried out on the data from each excitation wavelength (380 nm, 400 nm, and 550 nm) to fit the data to two, three, and four lifetimes. The kinetic trace and associate residuals for excitation at 380 nm (Figure S18), at 400 nm (Figure S19), and at 550 nm (Figure S20) are shown in the Supplementary Information. For all three excitation wavelengths, the fit residual improved going from two to three fitted lifetimes, although some residual structure remained in the three lifetime fit. However, addition of a fourth lifetime did not improve the residual, and the additional DADS produced in the global analysis had very low intensity suggesting that use of the fourth lifetime represented an overfitting of the data. Thus our observation is that the photophysical dynamics of **Pd[TPFPP]** do not vary with excitation wavelength, which is consistent with the typical paradigms for Pd(II) porphyrin photophysics.

Density functional theory picture of Pd[DMBil1] and Pd[TPFPP] photophysics. Density functional theory was employed to rationalize the origin of the distinct photophysics observed for the Pd(II) biladienes compared to the traditional **Pd[TPFPP]** moiety.

Ground state geometries. Initial optimizations of **Pd[DMBil1]** were performed using coordinates obtained from the published crystal structure of the same molecule.[32] This process resulted in a fully optimized (no imaginary frequencies) structure that was symmetric and fairly flat resembling that of a porphyrin. This geometry (GS'), which can also be obtained from an optimization of a 2D ChemDraw-adapted structure, is only *a local minimum* on the ground state surface (S_0). The global minimum (GS) that is 30 meV lower in energy has a bent biladiene backbone. Interestingly, the **Pd[MPBil1]**and **Pd[DPBil1]** complexes both crystalized in a very similar molecular orientation,[32] suggesting that this bent geometry is even more stabilized in the derivatives containing bulkier substituents at the sp^3-hybridized *meso*-carbon. The optimized GS' and GS structures are included within Figure 8.

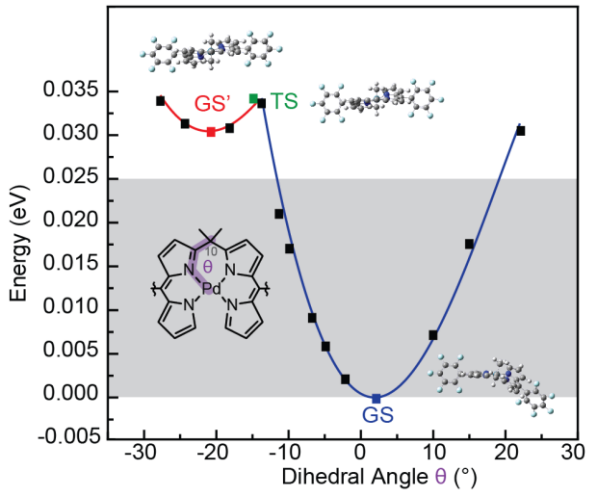

Figure 8. The ground state surface (S_0) and the two optimized minima (GS′ and GS) and the transition state between them (TS). Pd-N-C-C is the dihedral angle denoted as θ. Room temperature k_BT is shown in grey for reference. M06L/LANL2DZ[Pd]+6-311G(d,p)[H,C,N]/PCM(MeOH).

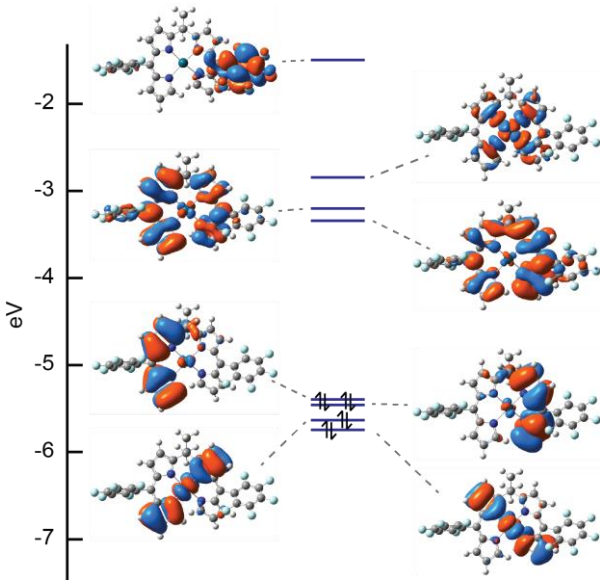

Figure 9. Molecular orbitals for **Pd[DMBil1]** GS configuration. M06L/LANL2DZ[Pd]+6-311G(d,p)[H,C,N]/PCM(MeOH).

All of the S_0 surface between the two minima is within 1.5 × k_BT at 298 K, such that we can expect the entire very flat S_0 surface to be populated. Despite the large ligand bend (Pd–N–C–C dihedral angle, θ, Figure 8), the two local ground-state minima possess very similar frontier molecular orbitals that differ only due to the broken symmetry in the GS due to the ligand bending (Figure 9, S6 and S8). Excited state and spin-orbit coupling analysis was performed for **Pd[DMBil1]** at both geometries (*i.e.*, GS' and GS) and the computed values deviate only slightly due to the similarities in the underlying orbitals of the

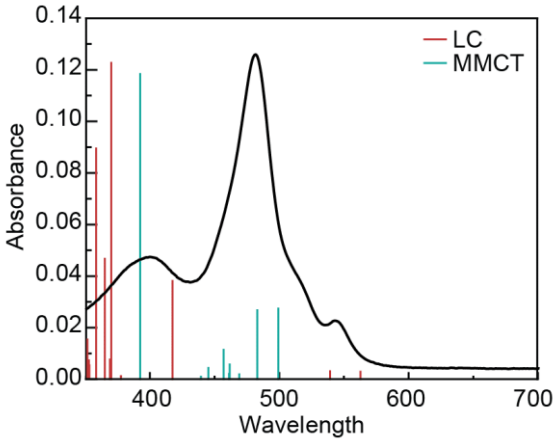

Figure 10. TDDFT excitations of **Pd[DMBil1]** GS overlaid with the experimental absorption spectrum of **Pd[DMBil1]**. Ligand-centered transitions are shown in black, and metal-mixed transitions in teal. States beyond S_{12} are shown in light grey. M06L/LANL2DZ[Pd]+6-311G(d,p)[H,C,N]/PCM(MeOH).

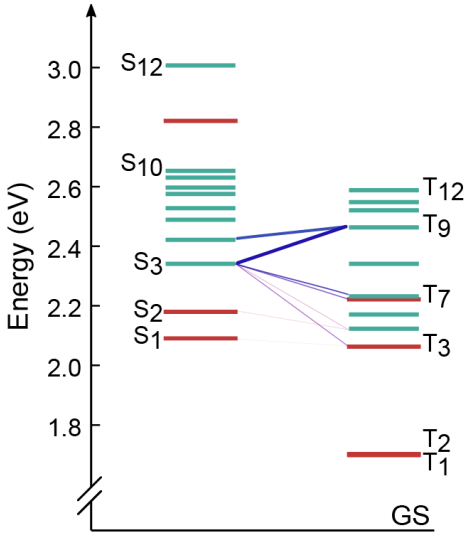

Figure 11. The singlet and triplet excited state manifolds at the GS geometry, ligand-centered states are black and metal-mixed states are teal. The strongest couplings between singlets in the experimental excitation window (2.2 eV for 570 nm excitation and 2.5 eV for the higher energy excitations) and the triplet manifold. SOCs are shown from red to blue, weakest to strongest, and with

confirmations. For the sake of clarity, we present the results of the true ground state (GS) herein and the full data for GS' is provided in the Supporting Information.

Time-dependent density functional theory. The calculated absorption spectra of **Pd[DMBil1]** (Figure 10) matches well with the experimental spectrum. The two lowest energy singlet excitations (592 nm and 567 nm) are mostly ligand-centered (LC), however the majority of higher energy excitations (390-500 nm) are metal-mixed charge transfer (MMCT) excited states. It is not possible to completely separate ligand-to-metal charge transfer (LMCT) and metal-to-ligand charge transfer (MLCT) transitions as the biladiene ligand is strongly mixed with the metal orbitals, indicating strong coupling similar to that which has been observed with strong σ-donating ligands.[47] Because of the strong coupling, each of the mostly metal-centered orbitals has contribution from the ligand, leading to the MMCT designation.

The triplets display a similar pattern (Figure 11) in that the lowest three (T_1–T_3) excited states are LC and most of the higher-energy states are MMCT. This ordering indicates that the higher-energy excitations may lead to MMCT triplet population. To untangle the multiple possible deactivation pathways in **Pd[DMBil1]**, we tracked the excited-state surfaces over a 60° rotation of the biladiene backbone ($-30° \leq \theta \leq 30°$, Figure S9) and calculated the spin-orbit couplings (SOCs) between the triplet and singlet states at both ground state minima and at the optimized triplet geometry (Tables S1–S6).

Spin orbit couplings. The SOCs show that for the lowest experimental excitation (2.2 eV or 570 nm) only the first two LC singlet states are populated. These states have fairly weak coupling into the triplet manifold, which leads to a relatively long (> hundreds of fs) singlet lifetime prior to ISC. Once the triplet state is formed, fast (< 10 ps) internal conversion means that during the first measured lifetime (τ_1), the excited state population should reach the lowest energy triplet (T_1). From T_1, there is weak coupling back to the ground state indicating a long-lived triplet should be observed, which aligns with the measured μs lifetime (τ_3) for **Pd[DMBil1]**.

For the higher energy excitation (2.5 eV, 490 nm), the initially populated excited singlet states (S_3–S_{12}) are mostly MMCT in character with strong direct coupling to the upper levels of the triplet manifold. The ~12 times stronger coupling of S_3 and S_4 to the T_9, than the S_1 to T_3 SOC, is consistent with fast ISC directly from the S_3 and S_4 states to the higher-energy triplet manifold, and bypassing of the expected $S_1 \rightarrow T_1$ evolution all together. This high energy ISC would result in a MMCT type triplet which undergoes internal conversion to the lowest energy triplet. Because the nature of the two triplets is quite different (T_9 versus T_1), the reorganization of the electron density and the correlated solvent reorganization should take on the order of hundreds of ps. The new lifetime seen in the higher energy excitation regime (τ_2 ~ 373 – 420 ps) fits well with this proposed high energy ISC and then triplet decay mechanism.

Once in the T_1 state, the long-lived triplet lifetime (τ_3) is observed due to the weak coupling back to the ground state. Importantly, the SOCs at GS' and at the optimized triplet geometry are very similar (Tables S1–S6) and the accessible excited-state energy surfaces of **Pd[DMBil1]** are extremely flat (Figure S9). This result is somewhat surprising given the extent of the rotation of the ligand explored but strongly suggests that the proposed photophysical scheme is expected to be similar along every point on the ground state surface.

DFT Summary of Pd[TPFPP]. The computational results obtained for **Pd[TPFPP]** are more straightforward, and are in line with what would be expected for the typical photophysics observed experimentally. The ground-state geometry shows one minimum due to the more rigid nature of the closed porphyrin macrocycle, with symmetric molecular orbitals as expected. The relative SOC into higher energy triplets (T_n, $n > 2$) vs T_1 are four times lower than those obtained for the Pd(II) biladienes (Tables S7 & S8) indicating that direct coupling into

the higher energy triplets states is not a dominate deactivation pathway in **Pd[TPFPP]**.

Implications for other Pd(II) biladienes. The computational results detailed above reveal that the twisted ground-state geometries of the Pd(II) biladienes drive the interesting photophysics that induce rapid ISC into the higher-energy triplet states upon higher-energy excitation. The crystal structures[32] and DFT optimizations of the biladienes bearing phenyl groups at the sp^3-hybrdized *meso*-carbon (*i.e.*, **Pd[MPBil1]** and **Pd[DPBil1]**) show that only the twisted geometry is a stable ground state minimum (*i.e.*, GS). These results are in contrast to the case for **Pd[DMBil1]**, which crystallized in the more planar configuration (*i.e.*, GS'). The DFT reveals that the excitations leading to the population of the higher-energy triplet excited state are dominated by the metal and the first coordination sphere. These results suggest that the higher-energy excited states of **Pd[MPBil1]** and **Pd[DPBil1]** should also have fast intersystem crossing into the higher-energy triplet states. The insights gained from this Pd(II) series serves a roadmap to enhance this effect in other biladiene and related tetrapyrole moieties.

Conclusions and Future Directions

Biladienes are non-aromatic oligotetrapyrroles that are related to porphyrins but which have breaks in the framework's π-conjugation due to the presence of an sp^3-hyrbidized *meso*-carbon at the 10-position and the non-macrocyclic nature of the architecture. Accordingly, biladienes are tetrapyrroles of much lower symmetry relative to traditional porphyrinoids and support interesting photochemical properties including the ability to strongly absorb light to induce population of long-lived triplet excited states (especially when complexed with Pd(II) or Pt(II). Up until this study, however, the excited-state dynamics of Pd(II) biladiene complexes have remained virtually unexplored.

In an effort to map the photophysics of these systems in detail, we embarked upon a comprehensive experimental and computational study of the excited-state dynamics on a series of 10,10-disubstituted Pd(II) biladiene derivatives. Through transient absorptions spectroscopy, we found that excitation into the lowest-energy absorption feature of the Pd(II) biladiene complexes shown in Figure 1 (representing excitation into the S_1 and S_2 states) results in typical photophysics, similar to what has been observed previously for Pd(II) porphyrins. More specifically, low energy excitation results in one lifetime on the picosecond time scale corresponding to singlet to triplet conversion, followed by a longer lifetime on the microsecond time scale corresponding to decay of the triplet state. Surprisingly, excitation into higher-lying excited states of the Pd(II) biladiene moieties using λ_{exc} = 350-500 nm light resulted in atypical photophysics in which a third lifetime is resolved. Further, unexpected emission excitation spectra bolster the observation that the Pd(II) biladienes support photophysics that are distinct from more traditional Pd(II) tetrapyrroles.

Density function theory was used to rationalize the origin of the third photophysical process observed upon higher-energy excitation and the unusual emission excitation spectra recorded for Pd(II) biladienes. In sum, lower-energy excitation of the Pd(II) biladienes results in population of ligand-centered excited states that give rise to standard Pd(II) tetrapyrrole photophysics, while higher-energy excitation results in population of charge-transfer excited states that possess significant spin-orbit coupling to higher-lying mixed-metal-charge-transfer (MMCT) triplet states (T_n, where n > 1). DFT calculations suggest that Pd(II) biladienes can readily undergo ISC directly to those higher-lying triplet states from the MMCT states. Accordingly, the photophysical scheme that emerges for Pd(II) biladienes is one in which higher-energy excitation into charge-transfer excited states results in dark states that deactivate through the lowest energy triplet back to the ground state (resulting in the unexpected emission excitation spectra that are observed). The relatively low symmetry of the biladienes (as compared to rigorously square planar porphyrins) leads to stronger interaction between the Pd(II) center and the tetrapyrrole ligand, which facilitates population of the low energy MMCT excited states in both the singlet and triplet manifolds leading to the interesting excitation-wavelength dependent photophysics. Notably, detailed, TAS, DFT, and excitation experiments show that the above phenomena are not operative for the analogous Pd[TPFPP] porphyrin complex, marking biladiene complexes as constructs that support photophysics distinct from those that have been thoroughly characterized for more common aromatic tetrapyrroles.

When taken together, the results of this study provide the first experimental and theoretical insight into the multi-facetted ultrafast dynamics of non-aromatic biladiene-based tetrapyrroles. This work provides an improved level of understanding into how the structural and electronic changes associated with breaking the aromaticity of tetrapyrrole complexes can impact the excited-state manifold and thereby the excited-state relaxation dynamics. More generally, the results of this work demonstrate that Pd(II) biladienes support a unique triplet photochemistry that may be exploited in future photochemical schemes and applications. Such efforts will be of continued interests in our laboratories.

Author contributions

Corresponding Author

* E-mail: ery317@lehigh.edu
* E-mail: laf218@lehigh.edu
* E-mail: joelr@udel.edu

Author Contributions

M.I.M., K.W., and T-N.P. synthesized biladiene and **Pd[TPFPP]** derivatives C.A.P. performed transient absorption data on the Pd(II) biladiene series, R.H. performed transient absorption on the **Pd[TPFPP]** and all emission spectroscopy. S.M.M. and G.R. performed DFT and TDDFT calculations. J.R., L.A.F. and E.R.Y designed the experiments and wrote the manuscript. The manuscript was edited through contributions of all authors. All authors have given approval to the final version of the manuscript.

Conflicts of interest

There are no conflicts to declare.

Associated content

Supporting Information. Additional fs-TA spectra with absorption spectra overlaid, as well as ns-TAS data and detailed global analysis results are found in the Supporting Information. DFT, TDDFT, and SOC details and tables are also found in the Supporting Information.

Acknowledgements

E.R.Y. thanks the NSF Major Research Instrumentation program for funds that established the multi-user laser facility for transient absorption (CHE-1428633). Portions of this research were conducted on Lehigh University's Research Computing infrastructure partially supported by NSF Award 2019035 and using the TG-CHE190011 allocation from Extreme Science and Engineering Discovery Environment (XSEDE), which is supported by National Science Foundation grant number ACI-1548562. Portions of the tetrapyrrole synthetic work were supported through the U.S. Department of Energy, Office of Science, Office of Basic Energy Sciences EPSCoR and Catalysis programs under Award Number DESC-0001234 (J.R.).

Notes and references

(1) Shi, Y.; Zhang, F.; Linhardt, R. J. Porphyrin-Based Compounds and Their Applications in Materials and Medicine. *Dye. Pigment.* **2021**, *188*, 109136.

(2) Milgrom, L. R. The Colours of Life: An Introduction to the Chemistry of Porphyrins and Related Compounds. *Q. Rev. Biol.* **2000**, *75*, 45–46.

(3) Flint, D. L.; Fowler, R. L.; LeSaulnier, T. D.; Long, A. C.; O'Brien, A. Y.; Geier, G. R. Investigation of Complementary Reactions of a Dipyrromethane with a Dipyrromethanemonocarbinol Leading to a 5-Isocorrole. *J. Org. Chem.* **2010**, *75*, 553–563.

(4) Costa, R.; Geier, G. R.; Ziegler, C. J. Structure and Spectroscopic Characterization of Free Base and Metal Complexes of 5,5-Dimethyl-10,15-Bis(Pentafluorophenyl)Isocorrole. *Dalt. Trans.* **2011**, *40*, 4384–4386.

(5) Hoffmann, M.; Cordes, B.; Kleeberg, C.; Schweyen, P.; Wolfram, B.; Bröring, M. Template Synthesis of Alkyl-Substituted Metal Isocorroles. *Eur. J. Inorg. Chem.* **2016**, *2016*, 3076–3085.

(6) Pomarico, G.; Xiao, X.; Nardis, S.; Paolesse, R.; Fronczek, F. R.; Smith, K. M.; Fang, Y.; Ou, Z.; Kadish, K. M. Synthesis and Characterization of Free-Base, Copper, and Nickel Isocorroles. *Inorg. Chem.* **2010**, *49*, 5766–5774.

(7) Thomas, K. E.; Beavers, C. M.; Gagnon, K. J.; Ghosh, A. β-Octabromo- and β-Octakis(Trifluoromethyl)Isocorroles: New Sterically Constrained Macrocyclic Ligands. *ChemistryOpen* **2017**, *6*, 402–409.

(8) Martin, M. I.; Cai, Q.; Yap, G. P. A.; Rosenthal, J. Synthesis, Redox, and Spectroscopic Properties of Pd(II) 10,10-Dimethylisocorrole Complexes Prepared via Bromination of Dimethylbiladiene Oligotetrapyrroles. *Inorg. Chem.* **2020**, *59*, 18241–18252.

(9) Cai, Q.; Tran, L.; Qiu, T.; Eddy, J.; Yap, G.; Rosenthal, J. An Easily Prepared Monomeric Cobalt(II) Tetrapyrrole Complex That Efficiently Promotes the 4e– /4H+ Peractivation of O2 to Water. *ChemRxiv* **2021**.

(10) Pistner, A. J.; Lutterman, D. A.; Ghidiu, M. J.; Ma, Y. Z.; Rosenthal, J. Synthesis, Electrochemistry, and Photophysics of a Family of Phlorin Macrocycles That Display Cooperative Fluoride Binding. *J. Am. Chem. Soc.* **2013**, *135*, 6601–6607.

(11) O'Brien, A. Y.; McGann, J. P.; Geier, G. R. Dipyrromethane + Dipyrromethanedicarbinol Routes to an Electron Deficient Meso-Substituted Phlorin with Enhanced Stability. *J. Org. Chem.* **2007**, *72*, 4084–4092.

(12) Kim, D.; Chun, H. J.; Donnelly, C. C.; Geier, G. R. Two-Step, One-Flask Synthesis of a Meso-Substituted Phlorin. *J. Org. Chem.* **2016**, *81*, 5021–5031.

(13) Pistner, A. J.; Yap, G. P. a; Rosenthal, J. A Tetrapyrrole Macrocycle Displaying a Multielectron Redox Chemistry and Tunable Absorbance Profile. *J. Phys. Chem. C* **2012**, *116*, 16918–168924.

(14) Pistner, A. J.; Lutterman, D. A.; Ghidiu, M. J.; Walker, E.; Yap, G. P. A.; Rosenthal, J. Factors Controlling the Spectroscopic Properties and Supramolecular Chemistry of an Electron Deficient 5,5- Dimethylphlorin Architecture. *J. Phys. Chem. C* **2014**, *118*, 14124–14132.

(15) Nieto-Pescador, J.; Abraham, B.; Pistner, A. J.; Rosenthal, J.; Gundlach, L. Electronic State Dependence of Heterogeneous Electron Transfer: Injection from the S1 and S2 State of Phlorin into TiO2. *Phys. Chem. Chem. Phys.* **2015**, *17*, 7914–7923.

(16) Allen J. Pistner, Maxwell I. Martin, Glenn P.A. Yap, J. R. Synthesis, Structure, Electronic Characterization, and Halogenation of Gold(III) Phlorin Complexes. *J. Porphyr. Phthalocyanines* **2021**, *25*, 683–695.

(17) Pistner, A. J.; Pupillo, R. C.; Yap, G. P. A.; Lutterman, D. A.; Ma, Y. Z.; Rosenthal, J. Electrochemical, Spectroscopic, And1O2 Sensitization Characteristics of 10,10-Dimethylbiladiene Complexes of Zinc and Copper. *J. Phys. Chem. A* **2014**, *118*, 10639–10648.

(18) Demchenko, A. P.; Heldt, J.; Waluk, J.; Chou, P.-T.; Sengupta, P. K.; Brizhik, L.; del Valle, J. C. Michael Kasha: From Photochemistry and Flowers to Spectroscopy and Music. *Angew. Chemie Int. Ed.* **2014**, *53*, 14316–14324.

(19) McGlynn, S. P.; Azumi, T.; Kasha, M. . External Heavy-Atom Spin — Orbital Triplet States. *J. Chem. Phys.* **1964**, *40*.

(20) Kee, H. L.; Bhaumik, J.; Diers, J. R.; Mroz, P.; Hamblin, M. R.; Bocian, D. F.; Lindsey, J. S.; Holten, D. Photophysical Characterization of Imidazolium-Substituted Pd(II), In(III), and Zn(II) Porphyrins as Photosensitizers for Photodynamic Therapy. *J. Photochem. Photobiol. A Chem.* **2008**, *200*, 346–355.

(21) Bogoeva, V.; Petrova, L.; Kubát, P. Binding of Palladium (II) 5, 10, 15, 20-Tetrakis (4-Sulfonatophenyl) Porphyrin to a Lectin for Photosensitizer Targeted Delivery. *J. Photochem. Photobiol. B Biol.* **2015**, *153*, 276–280.

(22) Obondi, C. O.; Lim, G. N.; D'souza, F. Triplet-Triplet Excitation Transfer in Palladium Porphyrin-Fullerene and Platinum Porphyrin-Fullerene Dyads. *J. Phys. Chem. C* **2015**, *119*, 176–185.

(23) Rice, A. T.; Yap, G. P. A.; Rosenthal, J. A P-61 Black Widow Inspired Palladium Biladiene Complex for Efficient Sensitization of Singlet Oxygen Using Visible Light. *Photochem* **2022**, *2*, 58–68.

(24) Potocny, A. M.; Riley, R. S.; O'Sullivan, R. K.; Day, E. S.; Rosenthal, J. Photochemotherapeutic Properties of a Linear Tetrapyrrole Palladium(II) Complex Displaying an Exceptionally High Phototoxicity Index. *Inorg. Chem.* **2018**, *57*, 10608–10615.

(25) Riley, R. S.; O'sullivan, R. K.; Potocny, A. M.; Rosenthal, J.; Day, E. S. Evaluating Nanoshells and a Potent Biladiene Photosensitizer for Dual Photothermal and Photodynamic Therapy of Triple Negative Breast Cancer Cells. *Nanomaterials* **2018**, *8*.

(26) Wang, J.; Potocny, A. M.; Rosenthal, J.; Day, E. S. Gold Nanoshell-Linear Tetrapyrrole Conjugates for near Infrared-Activated Dual Photodynamic and Photothermal Therapies. *ACS Omega* **2020**, *5*, 926–940.

(27) Rice, A. T.; Martin, M. I.; Warndorf, M. C.; Yap, G. P. A.; Rosenthal, J. Synthesis, Spectroscopic, and 1O2Sensitization Characteristics of Extended Pd(II) 10,10-Dimethylbiladiene Complexes Bearing Alkynyl-Aryl Appendages. *Inorg. Chem.* **2021**, *60*, 11154–11163.

(28) Baskin, J. S.; Yu, H. Z.; Zewail, A. H. Ultrafast Dynamics of Porphyrins in the Condensed Phase: I. Free Base Tetraphenylporphyrin. *J. Phys. Chem. A* **2002**, *106*, 9837–9844.

(29) Jäger, P.; Brendle, K.; Schwarz, U.; Himmelsbach, M.; Armbruster, M. K.; Fink, K.; Weis, P.; Kappes, M. M. Q and Soret Band Photoexcitation of Isolated Palladium Porphyrin Tetraanions Leads to Delayed Emission of Nonthermal Electrons over Microsecond Time Scales. *J. Phys. Chem. Lett.* **2016**, *7*, 1167–1172.

(30) Zamyatin, A. V.; Soldatova, A. V.; Rodgers, M. A. J. The Photophysics of Ni(II) Meso-Tetraphenylbenzoporphyrin: A Combined Theoretical and Experimental Investigation. *Inorganica Chim. Acta* **2007**, *360*, 857–868.

(31) Ryland, E. S.; Zhang, K.; Vura-Weis, J. Sub-100 Fs Intersystem Crossing to a Metal-Centered Triplet in Ni(II)OEP Observed with M-Edge XANES. *J. Phys. Chem. A* **2019**, No. Ii.

(32) Cai, Q.; Rice, A. T.; Pointer, C. A.; Martin, M. I.; Davies, B.; Yu, A.; Ward, K.; Hertler, P. R.; Warndorf, M. C.; Yap, G. P. A.; et al. Synthesis, Electrochemistry, and Photophysics of Pd(II) Biladiene Complexes Bearing Varied Substituents at the Sp3-Hybridized 10-Position. *Inorg. Chem.* **2021**, *60*, 15797–15807.

(33) Spellane, P. J.; Gouterman, M.; Antipas, A.; Kim, S.; Liu, Y. C. Porphyrins. 40. Electronic Spectra and Four-Orbital Energies of Free-Base, Zinc, Copper, and Palladium Tetrakis(Perfluorophenyl)Porphyrins. *Inorg. Chem.* **1980**, *19*, 386–391.

(34) Büttner, P.; Scheler, F.; Pointer, C.; Döhler, D.; Barr, M. K. S.; Koroleva, A.; Pankin, D.; Hatada, R.; Flege, S.; Manshina, A.; et al. Adjusting Interfacial Chemistry and Electronic Properties of Photovoltaics Based on a Highly Pure Sb2S3 Absorber by Atomic Layer Deposition. *ACS Appl. Energy Mater.* **2019**, *2*, 8747–8756.

(35) Gaussian 16, Revision B.01, M. J. Frisch, G. W. Trucks, H. B. Schlegel, G. E. Scuseria, M. A. Robb, J. R. Cheeseman, G. Scalmani, V. Barone, G. A. Petersson, H. Nakatsuji, X. Li, M. Caricato, A. V. Marenich, J. Bloino, B. G. Janesko, R. Gomperts, B. Mennu.

(36) Foresman, J. B.; Frisch. Exploring Chemistry With Electronic Structure Methods: A Guide to Using Gaussian. *Byte*. 1985, pp 239–242, 244, 246.

(37) Gao, X.; Bai, S.; Fazzi, D.; Niehaus, T.; Barbatti, M.; Thiel, W. Evaluation of Spin-Orbit Couplings with Linear-Response Time-Dependent Density Functional Methods. *J. Chem. Theory Comput.* **2017**, *13*, 515–524.

(38) Koseki, S.; Schmidt, M. W.; Gordon, M. S. Effective Nuclear Charges for the First- through Third-Row Transition Metal Elements in Spin-Orbit Calculations. *J. Phys. Chem. A* **1998**, *102*, 10430–10435.

(39) Khalil, G.; Gouterman, M.; Ching, S.; Costin, C.; Coyle, L.; Gouin, S.; Green, E.; Sadilek, M.; Wan, R.; Yearyean, J.; et al. Synthesis and Spectroscopic Characterization of Ni, Zn, Pd and Pt Tetra(Pentafluorophenyl)Porpholactone with Comparisons to Mg, Zn, Y, Pd and Pt Metal Complexes of Tetra(Pentafluorophenyl)Porphine. *J. Porphyr. Phthalocyanines* **2002**, *6*, 135–145.

(40) Schäferling, M. The Art of Fluorescence Imaging with Chemical Sensors. *Angew. Chemie - Int. Ed.* **2012**, *51*, 3532–3554.

(41) Borisov, S. M.; Klimant, I. Luminescent Nanobeads for Optical Sensing and Imaging of Dissolved Oxygen. *Microchim. Acta* **2009**, *164*, 7–15.

(42) Koren, K.; Borisov, S. M.; Klimant, I. Stable Optical Oxygen Sensing Materials Based on Click-Coupling of Fluorinated Platinum(II) and Palladium(II) Porphyrins - A Convenient Way to Eliminate Dye Migration and Leaching. *Sensors Actuators, B Chem.* **2012**, *169*, 173–181.

(43) Lee, S. K.; Okura, I. Photostable Optical Oxygen Sensing Material: Platinum Tetrakis(Pentafluorophenyl)Porphyrin Immobilized in Polystyrene. *Anal. Commun.* **1997**, *34*, 185–188.

(44) Yu, H.-Z.; Baskin, J. S.; Zewail, A. H. Ultrafast Dynamics of Porphyrins in the Condensed Phase: I. Free Base Tetraphenylporphyrin. *J. Phys. Chem. A* **2002**, *106*, 9837–9844.

(45) Chang, C. W.; Luo, L.; Chou, C. K.; Lo, C. F.; Lin, C. Y.; Hung, C. S.; Lee, Y. P.; Diau, E. W. G. Femtosecond Transient Absorption of Zinc Porphyrins with Oligo(Phenylethylnyl) Linkers in Solution and on TiO2 Films. *J. Phys. Chem. C* **2009**, *113*, 11524–11531.

(46) Imahori, H.; Kang, S.; Hayashi, H.; Haruta, M.; Kurata, H.; Isoda, S.; Canton, S. E.; Infahsaeng, Y.; Kathiravan, A.; Pascher, T.; et al. Photoinduced Charge Carrier Dynamics of Zn - Porphyrin - TiO2 Electrodes: The Key Role of Charge Recombination for Solar Cell Performance. *J. Phys. Chem. A* **2011**, *115*, 3679–3690.

(47) Fredin, L. A.; Wärnmark, K.; Sundström, V.; Persson, P. Molecular and Interfacial Calculations of Iron(II) Light Harvesters. *ChemSusChem* **2016**, *9*, 667–675.

TOC Graphic

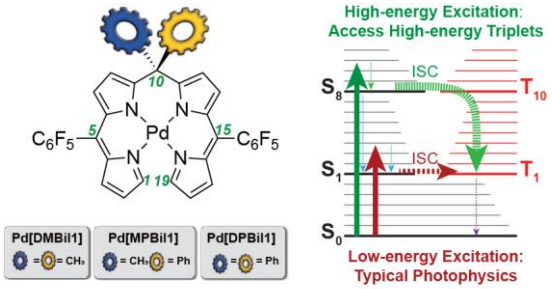

The *non-aromatic* nature of the 10,10-disubstituted Pd(II) biladiene backbone leads to atypical photophysics. Experiment and theory show that excitation into higher-energy mixed-metal singlet excited states can result in direct access to higher-energy triplet states not realized for traditional tetrapyrrole architectures.
